

AD-A246 269



1



National  
Defence

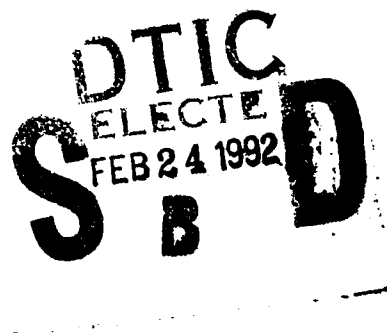
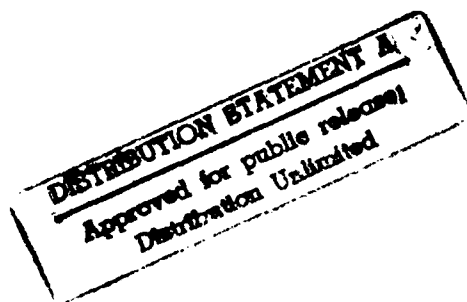
Défense  
nationale



# DESIGN OF DIGITAL SIGNAL PROCESSING ALGORITHMS FOR ENHANCING THE MEASUREMENTS OF ULTRA-FAST ELECTROMAGNETIC TRANSIENTS (U)

by

Marc Dion



**DEFENCE RESEARCH ESTABLISHMENT OTTAWA**  
REPORT NO. 1095

Canada

December 1991  
Ottawa

92-04393



92 2 19 097



National  
Defence

Défense  
nationale

# **DESIGN OF DIGITAL SIGNAL PROCESSING ALGORITHMS FOR ENHANCING THE MEASUREMENTS OF ULTRA-FAST ELECTROMAGNETIC TRANSIENTS (U)**

by

**Marc Dion**

*Nuclear Effects Section  
Electronics Division*

**DEFENCE RESEARCH ESTABLISHMENT OTTAWA**  
REPORT NO. 1095

PCN  
041LT

December 1991  
Ottawa

## ABSTRACT

This report describes the various techniques and algorithms developed to enhance the accuracy of the measurements of very fast transient electromagnetic fields generated during EMP testing. Some fundamentals of digital signal processing are presented and the practical aspects are highlighted. The response of some sensors to incident fields is studied. Appropriate algorithms for reconstructing the incident field from the measurements are developed. The effect of a low frequency cut-off of some sensors is also studied. A method to design a digital filter of arbitrary transfer function is presented. It is applied to compensate for losses occurring in long cables and also to fine tune other filters. The Hilbert transform is introduced to relate the magnitude and phase component of a transfer function. An implementation of the transform is given, allowing the design of digital filters when only the magnitude of the transfer function is known.

## RÉSUMÉ

Ce rapport décrit différentes techniques développées pour améliorer la précision des mesures de champ électromagnétique extrêmement rapide utilisés lors des tests d'impulsions électromagnétique (IEM). Certains aspects fondamentaux du filtrage numérique sont révisés. La réponse de capteurs à des champs électromagnétiques est étudiée. Différents algorithmes de filtrage pour obtenir le champ incident à partir des mesures sont conçus. Une méthode de conception de filtre numérique à fonction de transfert quelconque est présentée. Cette méthode est appliquée pour compenser l'atténuation des câbles et pour corriger les imperfections d'autres filtres. La transformée de Hilbert est utilisée pour établir une relation entre l'amplitude et la phase des fonctions de transfert. Cette relation permet de construire des filtres pour corriger des systèmes dont on ne peut mesurer que l'amplitude.

### EXECUTIVE SUMMARY

DREO has built a large experimental facility for the measurement of the effects of nuclear electromagnetic pulse (EMP) on systems. The transient field generated is extremely short and difficult to measure. This report describes the various techniques and algorithms developed to process and enhance these measurements.

The response of various sensors to incident fields is studied. It is shown that passive sensors normally respond to the time-derivative of the field, requiring some form of integration to recover the original field. Some well known methods are presented. An alternative technique is developed, based on both hardware and software. It is shown that the overall performances are improved and some experimental results are given. The effect of a low frequency cut-off of some sensors is also studied, and a correction algorithm is given.

A method to design a digital filter of arbitrary transfer function is presented. It is applied to compensate for losses occurring in long cables and also to fine tune other filters. The Hilbert transform is introduced to relate the magnitude and phase component of a transfer function. An implementation of the transform is given, allowing the design of digital filters when only the magnitude is known.



|                    |  |
|--------------------|--|
| Accession For      |  |
| NTIS GRA&I         | <input checked="checked" type="checkbox"/> |
| DTIC TAB           | <input type="checkbox"/>                   |
| Unannounced        | <input type="checkbox"/>                   |
| Justification      |  |
| By                 |  |
| Distribution/      |  |
| Availability Codes |  |
| Dist               | Avail and/or Special                       |
| A-1                |  |

## TABLE OF CONTENTS

|  | <u>PAGE</u> |
|--|-------------|
| ABSTRACT . . . . .   | iii         |
| EXECUTIVE SUMMARY . . . . .  | v           |
| TABLE OF CONTENTS . . . . .  | vii         |
| 1.0 <u>INTRODUCTION</u> . . . . .                                      | 1           |
| 1.1 THE EMP THREAT . . . . .   | 1           |
| 1.2 DREO LARGE EMP SIMULATOR FACILITY . . . . .                        | 2           |
| 2.0 <u>DIGITAL SIGNAL PROCESSING</u> . . . . .                         | 5           |
| 2.1 THE Z-TRANSFORM . . . . .  | 6           |
| 2.2 DESIGN OF IIR FILTERS . . . . .                                    | 9           |
| 2.3 DESIGN OF FIR FILTERS . . . . .                                    | 10          |
| 3.0 <u>CORRECTING FOR ELECTROMAGNETIC FIELD MEASUREMENTS</u> . . . . . | 13          |
| 3.1 INTEGRATING D-DOT AND B-DOT SENSORS OUTPUT . . . . .               | 15          |
| 3.2 COMPENSATING FOR LOW FREQUENCY CUT-OFF . . . . .                   | 21          |
| 4.0 <u>CORRECTING FOR MEASUREMENT SYSTEM ERRORS</u> . . . . .          | 25          |
| 4.1 CORRECTING FOR CABLE LOSSES . . . . .                              | 25          |
| 4.2 HILBERT TRANSFORM . . . . .  | 28          |
| 5.0 <u>CONCLUSION</u> . . . . .  | 35          |
| REFERENCES . . . . .   | 37          |

## **1.0 INTRODUCTION**

Under a program sponsored by DND, DREO is expanding its Nuclear Electromagnetic Pulse (EMP) research capability with the addition of a new large experimental facility. The EMP is a high-intensity, short-duration electromagnetic field that originates from a nuclear detonation. Although the energy content of EMP is not very large because of its short duration, electronic components or systems can be upset or damaged by the very high voltages or currents which can be induced. To assure EMP hardness, suitable tests and analysis are needed.

Even when the EMP hardening is taken into consideration from the beginning of the design stage and supported by prediction and analysis, a validation of such prediction by proper tests is necessary to raise the level of confidence. The EMP field or induced currents in cables or antennas are simulated and the system response is compared to the predictions.

DREO has built an EMP test facility in which a system under test is subjected to an EMP waveform. Measurements are made with a variety of sensors and probes, and good cables or fiber-optic links are used to carry these signals into a shielded-room housing all the sensitive data acquisition equipment. High speed digitizers must be used to record the extremely fast transient induced by the EMP waveform.

Sensors have their respective transfer function, data links introduce errors and instruments have their limitations, all of which alter the measurement being made. Post-processing of the data is necessary to remove errors and restore the original quantity that was measured (field or current). This report describes the various techniques and algorithms developed to process and enhance these measurements.

### **1.1 THE EMP THREAT**

The EMP produced by a nuclear burst at high altitude is a large-amplitude, very short duration transient field covering a very wide area beneath the burst point. In general, the exact characteristics of the EMP field such as peak amplitude, rise time and polarization, depend on many factors, such as the weapon yield, the height of burst and the observer's location. For practical purposes, a standard waveform representing a worst case is used [3] [4]. The standard EMP waveform has a peak value of 50 kV per meter, a rise time (10-90%) of about 4.2 nsec, a pulse width (50-50%) of about 185 nsec and a decay time (peak-to-10%) of about 600 nsec.

Two analytical expressions are commonly used to approximate the EMP waveform. The double exponential form (1), often referred to as the Bell curve [6] or the *old* NATO definition, is simpler and also has a simple Laplace transform, which makes it possible to solve simple problems analytically:

$$E(t) = AV \cdot (e^{-\alpha t} - e^{-\beta t}) \quad (1)$$

The reciprocal form (2), referred to as the *new* NATO definition, is more accurate as its derivatives are continuous over time, which gives a more realistic leading edge:

$$E(t) = AV \cdot \frac{e^{\alpha t}}{1 + e^{(\alpha + \beta)t}} \quad (2)$$

## 1.2 DREO LARGE EMP SIMULATOR FACILITY

DREO has designed and built a large bounded wave EMP simulator of about 100 meters long, 20 meters wide and 10 meters high with a useful working area of 30 by 20 meters. Bounded wave simulators produce electromagnetic fields confined between two parallel plates or between wire arrays approximating two parallel plates. The plates are tapered at both ends with a generator attached at one end and a terminating load at the other end. This type of simulator is in fact a large transmission line with a fairly uniform field within the parallel section. The generator is capable of launching a 600 kV impulse with a 5 ns rise time in the transmission line necessary to produce the 50 kV/m fields required by the MIL-STD-461C standard.

The system response is measured by field sensors and current or voltage probes. Field sensors are generally passive devices, basically electric dipole or magnetic loop. Their response can be very fast with a high dynamic range, but their sensitivity is relatively low. Their output is generally the time-derivative function of the field (known as D-dot and B-dot sensors) which will require further processing to restore the waveform and for D-dot sensors, the output voltage can be expressed by:

$$V_o = R \cdot \vec{A}_{eq} \cdot \frac{d\vec{D}}{dt} = R \cdot A_{eq} \cdot \frac{dD}{dt} \cdot \cos \theta \quad (3)$$

High speed digitizers are used to convert the measurements into digital form. A number of them are used, at present allowing up to a total of nine simultaneous measurements. The table below summarizes the key characteristics of each. These instruments give the capability of measuring transients (single shot) with a rise time shorter than 1 or 2 nanoseconds. Due to the limited number of samples obtained at the faster rates (> 1 Gs/sec), it is not always

possible to capture the whole signal, which may last more than 1-2  $\mu$ s, and still capture accurately the fast rising edge (few nanoseconds). Two channels, at different speeds, may be used to record the whole signal.

| Model        | Bandwidth | Sampling rate |
|--------------|-----------|---------------|
| SCD1000      | 1 GHz     | 200 G·s/sec   |
| TEK7912HB    | 700 MHz   | 100 G·s/sec   |
| DSA602       | 400 MHz   | 2 G·s/sec     |
| LeCroy 6880A | 400 MHz   | 1.3 G·s/sec   |
| LeCroy 8828C | 100 MHz   | 200 M·s/sec   |

The recorded data is transferred to a computer for storage and post-processing. It is very important to save along with the measurements all the information necessary to identify the setup used for the test and all the instrument parameters necessary to reconstruct the waveform.

Data processing of the waveforms is an essential part of the measurement process. It is possible to model arbitrary transfer functions and to compensate for errors, such as:

- recover from a sensor transfer function (by differentiation, integration, scaling, etc.)
- account for sensor calibration
- compensate for cable attenuation at higher frequencies
- account for any attenuator or filter inserted
- compensate for some of the instrument limitations
- merge two measurements of the same signal
- perform functions on multiple measurements (averaging, dejitter, etc.)



## 2.0 DIGITAL SIGNAL PROCESSING

Digital signal processing (DSP) is the digital counterpart of analog filtering. Algorithms to be applied onto digitized signals are designed to approximated the desired filtering functions. Digital filters may be real time, in which case their output is converted back to analog signals, or they may operate on pre-stored data sequences of finite length. The transfer function of the digital filter can be precisely tailored and, contrary to its analog equivalent, is not affected by tolerance or variation of components.

In the discrete-time linear systems theory, from which digital processing is derived, signals are defined only for the discrete values of time  $t = n \cdot T$ , where  $T$  (also often denoted as  $\Delta t$ ) is the interval between samples. Discrete-time signals are represented as sequences of numbers. Related to the analog world, a sequence may represent an analog signal sampled at a regular interval. A sequence is denoted  $\{x\}$  and the  $n^{\text{th}}$  element of it as  $x(n)$  or  $x_n$ . Sequences may be infinite or have a finite number of samples  $N$  ( $x_0$  to  $x_{N-1}$ )

The most straightforward approach to compute the response of a system is to multiply the input and the transfer function in the frequency domain:

$$\begin{array}{ccc} e(t) \Rightarrow E(\omega) & & \\ \cdot & & \\ H(\omega) & & (4) \\ \Downarrow & & \\ y(t) \Leftarrow Y(\omega) & & \end{array}$$

and use a fast Fourier transform (FFT) algorithm to generate the time domain response. This approach has several drawbacks.  $e(t)$  and  $H(\omega)$  must have the same size, which must be a power of 2 in order to use the standard FFT algorithm. Although the FFT is efficient to compute the spectrum of a signal, it is not the most efficient approach to filtering, specially for longer sequences (some of the digitizers may record as many as 64,000 data points).

The FFT has also some *side-effects*, which may alter the solution considerably. Consider for instance a measurement truncated in order to obtain details of the rising edge. This truncation will introduce a severe aliasing in the solution. This aliasing is caused because taking the inverse FFT of a product corresponds to performing a circular convolution in time domain. This problem can be eliminated if both sequences are doubled by adding zero's, which would then corresponds to performing a linear convolution. This however is at the expense of an increase of the compute time and storage area by a factor of 4. Nonetheless, truncating a sequence is equivalent to multiplying it with a rectangular window, which corresponds to the convolution of  $H(\omega)$  with a  $\text{sinc}(x)$

function. This is the well-known Gibbs phenomenon, which causes  $H(\omega)$  to ripple and overshoot by as much as 9% around discontinuities and rapid transitions.

A better approach to perform digital filtering is the use of the z-transform, based on the theory of discrete-time linear systems.

## 2.1 THE Z-TRANSFORM

In continuous-time systems theory, we use the Laplace and the Fourier transforms to characterize linear time-invariant systems. Similarly, it is possible to generalize these transforms for discrete-time systems, resulting in the z-transform.

The transform  $X(Z)$  of a sequence  $x(n)$  is defined as:

$$X(z) = \sum_{n=-\infty}^{\infty} x(n) z^{-n} \quad (5)$$

where  $z$  is a complex variable. The function will converge only for some values of  $z$ . Detailed discussion of the z-transform can be found in [7], but we can state the general results for our cases of interest. The series will converge for values of  $z$  on the unit circle if the system is stable, and vice-versa. The z-transform will always converge on the unit circle for finite-length sequences and will converge for causal sequences if all the poles of the transform lie inside the unit circle.

The z-transform may be related to the Fourier transform by evaluating it on the unit circle, ie. by using the relation:

$$z = e^{j\omega} \quad (6)$$

in (5) above, yielding to:

$$X(z) \Big|_{z=e^{j\omega}} = X(e^{j\omega}) = \sum_{n=-\infty}^{\infty} x(n) e^{-j\omega n} \quad (7)$$

which is the Fourier transform of  $x(n)$ . This relation is important as it gives the exact frequency response of a digital filter with a transfer function  $H(z)$ . Similarly, the z-transform may also be related to the Laplace transform with the substitution:

$$z = e^{sT} \quad (8)$$

Not surprisingly, the z-transform shares the same basic properties of the Laplace and Fourier transforms. The z-transform is linear; that is the transform of  $ax_1(n) + bx_2(n)$  is  $aX_1(z) + bX_2(z)$ .

One of the most important and useful property is the shift in time (delay) of a sequence. If a sequence  $x(n)$  is delayed by  $n_0$  samples, then the following relation is obtained:

$$x(n-n_0) \rightleftharpoons z^{-n_0} X(z) \quad (9)$$

where  $z^{-n_0}$  can be seen as a delay element, similar to  $e^{-t_0 s}$  with the Laplace transform and  $e^{-j\omega t_0}$  with the Fourier transform.

As with the Laplace transform, it can be shown that the multiplication of two z-transforms corresponds to the convolution of the two corresponding sequences, i.e.:

$$x(n) * y(n) \rightleftharpoons X(z) Y(z) \quad (10)$$

where the convolution is defined by:

$$x(n) * y(n) = \sum_{k=-\infty}^{\infty} x(k) y(n-k) \quad (11)$$

Furthermore, the input-output relation of a system corresponds to the multiplication of the z-transforms of the input and the unit-sample response, in a way similar to the Fourier transform as expressed by (4). This property suggest that one could use the same method for solving problems. It would require performing the z-transform of the input with (5) and an inverse transform of the output (not shown, but it is a rather complicated function, difficult to calculate). Instead, if we define  $H(z)$  as a ratio of two polynomials in  $z^{-1}$  such as:

$$H(z) = \frac{B(z)}{A(z)} = \frac{\sum_{j=0}^M b_j z^{-j}}{\sum_{k=0}^N a_k z^{-k}} \quad (12)$$

and if we apply the delay property to (5), we obtain:

$$\sum_{k=0}^N a_k y(n-k) = \sum_{j=0}^M b_j x(n-j) \quad (13)$$

which may be normalized for  $a_0=1$  and rewritten as<sup>1</sup>:

$$y_n = b_0x_n + b_1x_{n-1} + b_2x_{n-2} + \dots b_Mx_{n-M} - a_1y_{n-1} - a_2y_{n-2} - \dots a_Ny_{n-N} \quad (14)$$

which states that the output at a given time  $n$  is a function of the present and past values of the input, and also a function of the past values of the output. The problem of designing a filter of given characteristics becomes a question of finding the proper coefficients.

All the algorithms developed in this report are based on the relations between the  $z$ -transform and the Fourier and Laplace transforms and the use of several techniques to transpose a transfer function from the frequency domain or the  $s$ -domain into the  $z$ -domain to obtain  $H(z)$ . Relation (14) provides an efficient computer implementation of the resulting filter.

Several techniques have been developed to design digital filters, yielding to two general classes of filters. For filters where  $A(z)$  is 1 ( $a_0$  is 1, all other terms are 0), the output depends on the input only and consequently the impulse response of such system will be of finite duration. Such filters are known as Finite Impulse Response (FIR) filters. For cases where the output may also depend on the past values of the output, the impulse response is infinite because of the recursive nature of these filters. These filters are known as Infinite Impulse Response (IIR) filters. FIR and IIR filters each have their advantages and disadvantages and the choice between one or another and the technique used to find the coefficients is often dictated by the particular problem:

- IIR filters are the most efficient, requiring 5 to 10 times fewer coefficients than the FIR equivalent.
- IIR filters are primarily limited to more classical filters, such as low-pass, high-pass, pass-band, band-stop, etc., for which the expression in Laplace domain is known. It also allows the use of the classical solutions of filter design, such as Butterworth, Chebyshev, elliptic filters.
- An expression for calculating the coefficients of IIR filters for any  $\Delta T$  can usually be obtained. By comparison, the coefficients of FIR filters are often obtained by iterative or cumbersome procedures and are calculated for a single  $\Delta T$  only, therefore requiring the

---

<sup>1</sup> A detailed development of this relation can be found in [7].

storage in advance of tables containing the coefficients of various  $\Delta T$ .

- FIR filters can be designed to have a precisely linear phase, which is not possible with IIR filters.
- FIR filters can be designed to match any arbitrary response.

## 2.2 DESIGN OF IIR FILTERS

Designing a digital filter (ie. finding the proper coefficients) is basically a problem of approximating the characteristics of the desired filter by following some criteria. IIR filters are best suited for cases where an equivalent analog filter exists. Several techniques (such as the impulse invariance, mapping of differential equations, the bilinear transformation, and the matched  $z$  transformation) have been developed to transpose a filter defined in  $s$ -domain into the  $z$ -domain. Of particular interest to our application is the bilinear transform.

This procedure is developed in [7] by solving a simple problem with the integral equation and approximating the integral with the trapezoidal rule, resulting in the substitution<sup>1</sup>:

$$s = \frac{2}{T} \frac{1-z^{-1}}{1+z^{-1}} \quad (15)$$

The main advantages of the bilinear substitutions are:

- A  $N^{\text{th}}$  order transfer function  $H(s)$  gives a  $N^{\text{th}}$  order digital filter, thus simple filters will result into simple equations.
- A stable analog filter will always give a stable digital filter.
- The transformation does not introduce aliasing. Therefore, it is possible to design filters operating near their Nyquist limit.

There is however one disadvantage, that is the introduction of a distortion of the frequency axis. The relation between the analog frequency  $\Omega$  and the digital frequency  $\omega$  is no longer linear, but corresponds to:

---

<sup>1</sup> This expression is also an approximation of (8), ie. the truncation to one term of the Taylor series expansion of  $s = \ln z / T$ .

$$\frac{\omega T}{2} = \tan^{-1}\left(\frac{\Omega T}{2}\right) \quad (16)$$

which may be considered linear for low frequencies and the distortion will grow as the frequency approaches the Nyquist frequency. For instance, for  $\Omega_c = 1/10$ ,  $1/4$  and  $1/2$  of the Nyquist frequency, the distortion is 1%, 5% and 15% respectively. In many cases, this distortion may be accounted for. Consider for instance the design of a low-pass or band-pass filter with a critical cut-off frequency  $\Omega_c$ . It is possible to still obtain a very acceptable filter with the bilinear transformation by solving the problem for the cut-off frequency  $(2/T)\tan(\omega_c T/2)$  instead of  $\omega_c$ , ie. by pre-distorting the frequency axis.

### 2.3 DESIGN OF FIR FILTERS

FIR filters are attractive particularly for their capability to implement arbitrary frequency responses. As seen, the transfer function of a FIR filter is given as:

$$H(z) = \sum_{n=0}^{N-1} h(n) z^{-n} \quad (17)$$

where  $h(n)$  is the impulse response of the filter. A FIR filter is designed simply by finding its impulse response<sup>1</sup>. However, in most cases, the impulse response is infinite, ie. it extends from  $-\infty$  to  $+\infty$ . The most straightforward approach consists of truncating the impulse response to  $N$  terms. This truncation, however, leads to the well-known Gibbs phenomenon. Simply, truncation in time domain is similar to a multiplication with a rectangular window and results in frequency domain in the convolution of  $H(z)$  with the transform of the window, which is  $\sin(\omega N/2)/\sin(\omega/2)$ . The result is a smear of the frequency response, especially near the sharp transition, resulting in a fixed percentage of overshoot and ripple. For example, the overshoot of an ideal low-pass filter is about 9% at the transition, and more important, it does not decrease as the size of  $h(t)$  is increased. The problem may be controlled with the use of other windows, such as the Hamming, Hanning, Blackman, Bartlett and Kaiser windows. These windows increase the stop-band attenuation and decrease the main lobe width, resulting in smaller overshoot and a more abrupt stop band. This, however, is at the cost of a larger  $N$ . In our applications, where we are concerned about compensating for cable losses, etc., the frequency response is fairly smooth and thus, the Gibbs effect is very small and may be neglected.

---

<sup>1</sup> Another technique, known as the frequency-sampling, allows to design FIR filters by specifying  $N$  samples of their frequency response. This design is particularly attractive for narrow pass-band filters, but in general the windowing techniques are more practical and more flexible.

Ideally, the analytical form of  $h(n)$  should be used to calculate the coefficients. In many cases, it is difficult to evaluate and a  $M$ -point inverse DFT or FFT is used with a  $N$ -point window. This gives accurate results, especially if the frequency response is smooth and if  $M \gg N$ . However, great care should be exercised to avoid the side-effects resulting from the application of the DFT algorithm. In any case, relation (6) should be used to check the response of the filter, specially for frequencies not a multiple of  $\Delta f$  as the filter may give an exact solution for these frequencies but exhibit some ripple for others. A technique for designing FIR filters will be further developed in Chapter 4.

Some problems are more difficult (or impractical) to implement as FIR filters because their impulse response is of long duration and would require a large number of points. Consider for instance a 1<sup>st</sup> order low-pass filter with a cut-off frequency  $\omega_c = 0.01/T$ . Its impulse response is  $\exp(-\omega_c nT)$  and between 250 and 500 samples would be required to create a FIR filter. Filters which exhibit resonances (narrow band filters) also have a long duration impulse response. On the other hand, filters with a near unity frequency response, such as one designed to compensate for the slight loss occurring in cables at higher frequencies, have a very short impulse response<sup>1</sup>, resulting in typically between 5 to 20 coefficients.

This last property can be used to combine both FIR and IIR techniques to design more efficient filters. Consider for instance the problem shown on Figure 2-1 where the desired function  $H(\omega)$  cannot be expressed easily in the  $s$ -domain. A FIR design would give a very good approximation of the function, but with a large number of coefficients. Instead,  $H(\omega)$  can be represented as the product two functions:  $G(\omega)$  being an ideal 1<sup>st</sup> order low-pass filter, and  $E(\omega) = H(\omega)/G(\omega)$  being the error between the two.  $G(\omega)$  is efficiently implemented as a 1<sup>st</sup> order IIR filter and  $E(\omega)$  as a FIR filter with few coefficients. This results obviously in an IIR filter.

---

<sup>1</sup> The impulse response of a pass-all filter,  $H(\omega) = 1$ , is the ideal impulse  $\delta(n)$ . Consequently, the impulse response will tend toward the ideal impulse as the frequency response approaches unity.

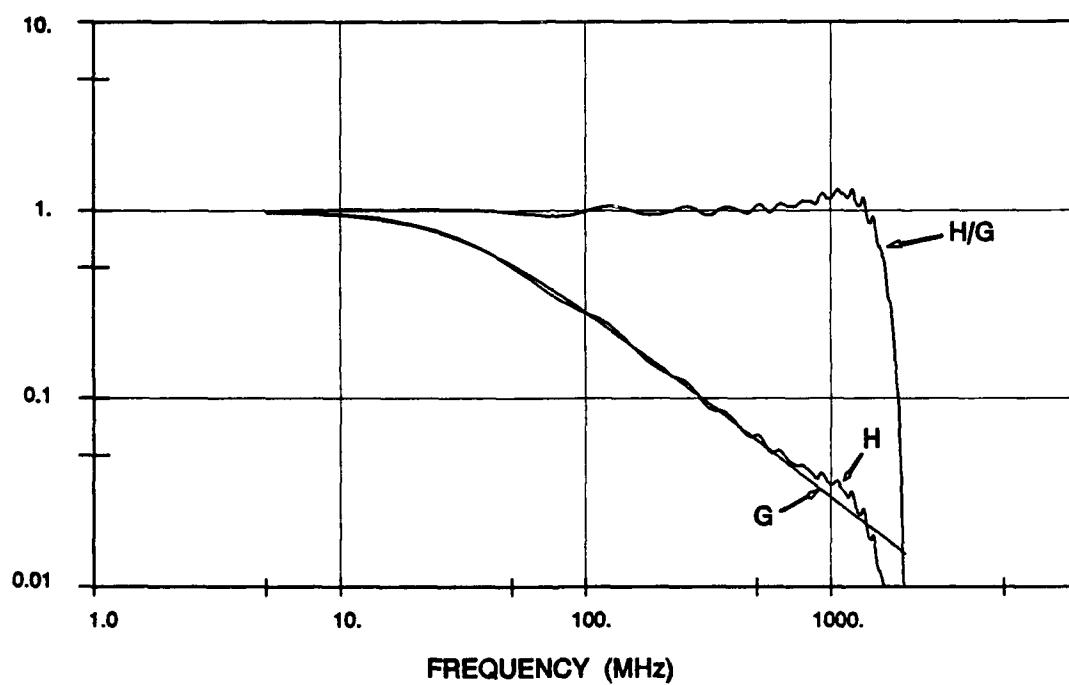


Figure 2-1. Using a FIR filter to fine tune an IIR filter.



### 3.0 CORRECTING FOR ELECTROMAGNETIC FIELD MEASUREMENTS

Field sensors are used to measure the electric field ( $E$ , in Volt/meter) or flux density ( $D = \epsilon_0 E$ , in Coulomb/meter, where  $\epsilon_0 = 8.85 \cdot 10^{-12}$ ) and the magnetic field ( $H$ , in Ampere/meter) or flux density ( $B = \mu_0 H$ , in Tesla, where  $\mu_0 = 4\pi \cdot 10^{-7}$ ). Field sensors may be active or passive (ie. no external power), but generally passive devices are used. The most basic type of field sensor is the small<sup>1</sup> electric dipole or the small magnetic dipole (loop).

Figure 3-1 shows a simple circuit model for a small electric and a small magnetic dipoles. The transfer function of the electric dipole is given as:

$$V_{out} = h_{eq} \cdot \frac{RCs}{1 + RCs} \cdot E \cos \theta = A_{eq} R \cdot \frac{s}{1 + RCs} \cdot D \cos \theta \quad (18)$$

which both output a voltage proportional to the normal component of the field ( $\theta$  being the angle between the field and vector normal to the sensor ground plane) above a certain cut-off frequency (related to the time constants  $RC$  and  $L/R$ ), and a voltage proportional to the time-derivative of the field below it. For practical geometries and for sensors normally matched to the instrumentation ( $50 \Omega$ ), these sensors operate well below the cut-off frequency and thus will always respond to the derivative of the field, approximated by:

$$V_{out} \approx A_{eq} R \cdot \frac{dD}{dt} \cos \theta \quad (19)$$

Similarly, the output of the magnetic dipole, is given by:

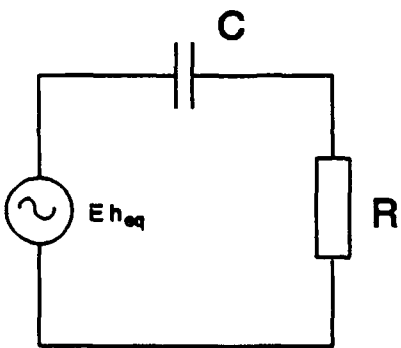
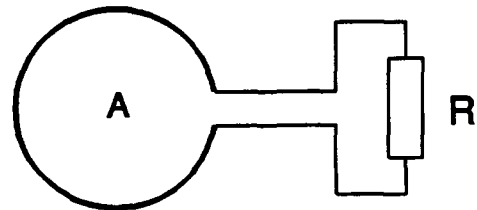
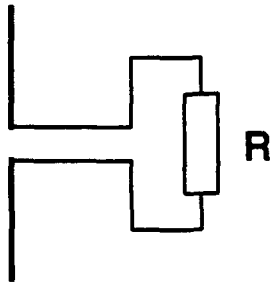
$$\begin{aligned} V_{out} &= \mu A \frac{R}{R + Ls} \cdot \frac{dH}{dt} \cos \theta = A_{eq} \frac{s}{1 + \frac{L}{R}s} \cdot B \cos \theta \\ &\approx A_{eq} \cdot \frac{dB}{dt} \cos \theta \end{aligned} \quad (20)$$

Because these sensors output the time-derivative of the excitation, they are known as  $\dot{D}$  and  $\dot{B}$  sensors (or  $\dot{D}$  and  $\dot{B}$  sensors). Since the response of these sensors depend on the geometry and the external load only, accurate calibration can be obtained from the sensor dimensions solely.

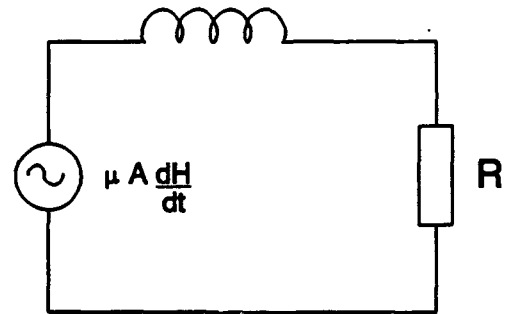
It is obviously necessary to perform an integration on  $\dot{D}$  and  $\dot{B}$  sensors output to restore the original field waveform. Section 3.1 will present several methods to achieve integration. Section 3.2 will discuss the case of a

---

<sup>1</sup> Small is define as electrically small, relative to the wavelength of highest frequency. For standard EMP waveform, it corresponds to sensors smaller than 10-15 cm.



Electric dipole model



Magnetic dipole model

Figure 3-1. Simple models of electromagnetic field sensors.

small short-circuited loop used to measure the H field directly.

### 3.1 INTEGRATING D-DOT AND B-DOT SENSORS OUTPUT

Two traditional and straightforward methods have been used to integrate the measurements of D-dot sensors<sup>1</sup>: using software integration and using hardware integration. A better method combining the advantages of both will be presented in this section.

This simplest of all methods is to digitize the raw data from the sensor and perform the integration by software with the simple algorithm:

$$Y_n = Y_{n-1} + X_n \quad (21)$$

This technique works well, but it has major disadvantages. Because the D-dot sensors respond to the time-derivative, they produce an output which is even faster than the excitation. Figure 3-2 (top) shows in (a) a typical D-dot measurement with a rise time of approximately 1.2 ns, which is about 5 times faster than the actual field being measured as shown on bottom<sup>2</sup>. It is therefore necessary to oversample the signal to capture the faster rising edge. An other major problem with this technique is the reduction of the dynamic range resulting in a poorer resolution of the part of the signal corresponding to the falling edge of the pulse (this problem will be discussed later). This algorithm is also highly susceptible to the trigger jitter unless a sufficient number of points is obtained on the rising edge. Of course, this technique also requires higher bandwidth instrumentation and data links, which becomes very expensive at frequencies above 1 GHz.

The other common technique to integrate the measurement, is the use of a passive integrator. They consist of simple resistor-capacitor passive network resulting in a 1<sup>st</sup>-order low-pass filter with the transfer function:

$$H(s) = \frac{1}{1 + \tau s} \quad (22)$$

which approximate an integrator for frequencies large compared to  $1/\tau$ . For commonly available devices ( $\tau = 1$  to  $10 \mu\text{sec}$ ), the rising edge will be properly restored and consequently, there is no need to oversample as the signal being

---

<sup>1</sup> This section also applies to B-dot magnetic sensors.

<sup>2</sup> Actually, the reference curve shown is the voltage measured across the two plates of the simulator near the generator. This voltage is faster than the actual field found at the sensor location, which is about 6.5 ns.

measured is not much faster than the original field. On the other hand, the falling edge will sag due to the cut-off frequency in the range of 30-300 kHz, and will need to be restored with further processing. A disadvantage of these devices is that they are designed to match high-impedance ( $1\text{ M}\Omega$ ) instrumentation, which is not usual for high-bandwidth digitizers<sup>1</sup>. But the biggest disadvantage is their high insertion loss. The output of a D-dot sensor to a 40 kV/m field is about 25 Volt peak, and the output of a 1  $\mu$ sec integrator is 75 mV peak. It then becomes impossible to measure lower fields, such as in boxes or enclosures.

An alternate technique developed to overcome these disadvantages make use a specially designed device similar to the passive integrator, but with a much smaller time constant of the order of 2 to 10 ns, that has been named a partial integrator. The result is that only the higher frequencies which contribute for the accelerated rise time are integrated. The output still needs to be processed, but it is only 10 to 50% faster than the original field, making it easier to digitise. The effect of such a device can be observed on Figure 3-2 (top), where the curve (b) is the output of a 5 ns partial integrator. The sensor output is slowed to give a rise time of about 4.1 ns, thus allowing the use of a slower sweep to capture a longer time window.

Another advantage of the passive integrator is the increase in dynamic range. The time-derivative of the field result in a signal of large amplitude during the short rising portion of the field, followed by a much smaller signal (in this example, with an amplitude of  $1/25^{\text{th}}$  of the peak) of long duration during the decay portion. The digitizers have a resolution of 8 to 9 bits for a full scale signal necessary to capture the peak amplitude, leaving a resolution of only about 4 bits for the trailing edge. This poor resolution will introduce noticeable errors during the integration. In this example, the 5 ns partial integrator reduces the peak amplitude by only 40%, but a 30 ns partial integrator would reduce the amplitude by a factor of 5, resulting in an increase in dynamic range of about 2 or 3 bits.

To build even a simple filter for frequencies above 100 MHz is difficult. Discrete components cannot be used because of stray capacitance of inductors and stray inductance of leads and capacitors. Even very short leads introduce stub effect. This problem has been addressed by designing a transmission line section about 5 inches long. The diameter of the central conductor and the outer shell are about 0.312 and 0.718 inches respectively and are chosen to maintain the 50  $\Omega$  characteristic impedance. The middle portion of the central conductor is made much thicker, almost touching the outer shell, thus inserting a relatively large capacitance. This conductor is made of aluminum which is anodized to form a very

---

<sup>1</sup> The LeCroy digitizers have a front-end amplifier, which may be used to provide a high impedance input, but at the cost of limiting the bandwidth to 150 MHz.

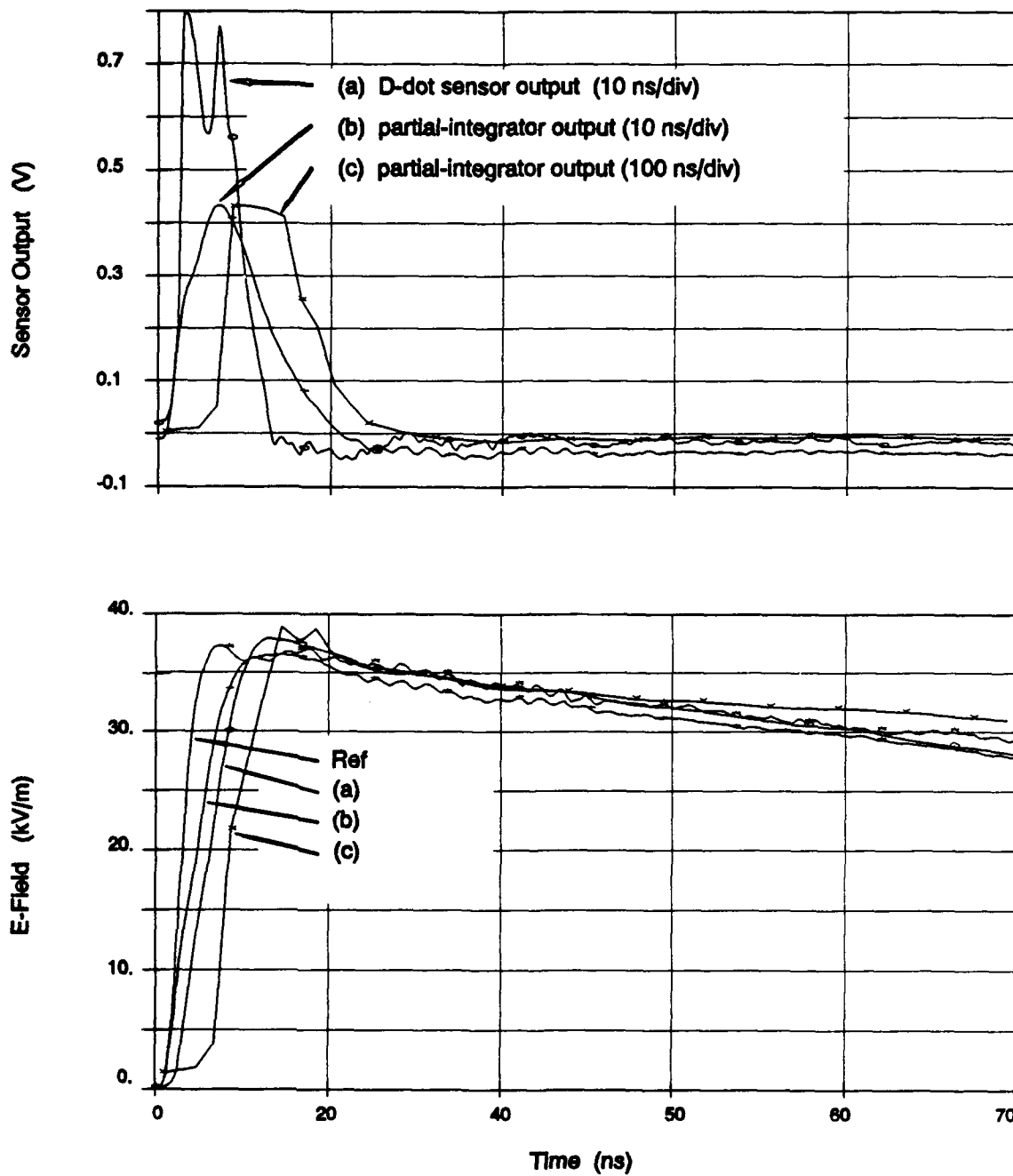


Figure 3-2. Comparison of a D-dot sensor output and a partial-integrator output.

good insulating layer at the surface to prevent any conduction to the outer shell. This capacitance ( $C_x$ ) appears in parallel with the load and values in the range of 100 to 400 pF can be obtained. This capacitance is much larger than the internal capacitance  $C$  of the sensor, changing its transfer function to:

$$V_{out} = A_{eq} R \frac{dD}{dt} \cos\theta \cdot \frac{1}{1 + RC_x s} \quad \text{for } C_x \gg C \quad (23)$$

which is equivalent to the sensor output passed through a 1<sup>st</sup>-order filter with a cut-off frequency  $f_c$  of  $1/2\pi RC_x$ . It is difficult to build the device to match a given  $f_c$ , but as long as the transfer function can be measure accurately, proper waveform recovery can be achieved. Figure 3-3 shows the measured transfer function of a partial integrator compared with an ideal 1<sup>st</sup>-order low-pass filter, with at cut-off frequency of 30 MHz. The agreement is very good: less than 1 dB deviation for frequencies up to 750 MHz, making it suitable for an IIR implementation<sup>1</sup>.

Recovery of the original field is done simply by multiplying  $V_{out}$  by  $(1 + RC_x s)$  to undo the effect of the partial integrator ( $C_x \approx 100$  pF), and then multiply by  $1/s$  to integrate. By using the bilinear transformation, we obtain the transfer function:

$$H(z) = \frac{(\frac{T}{2} + RC_x) + (\frac{T}{2} - RC_x) z^{-1}}{1 - z^{-1}} \quad (24)$$

which translates to:

$$y_n = y_{n-1} + (\frac{T}{2} + RC_x) x_n - (\frac{T}{2} - RC_x) x_{n-1} \quad (25)$$

On Figure 3-2 (bottom), the result of this algorithm is shown on curve (b). The agreement with a purely software integration on curve (a) is very good. The algorithm is very stable, as it can be seen on curve (c), where the sweep rate was selected to be very near the Nyquist limit (sampling at about every 2 ns). The key characteristics of the field (rise time, peak amplitude) and the overall shape of the curve is still very close to the other measurements (done at a 0.2 ns sampling rate), even when severe blooming occur onto the internal graticule of the digitizer such as in this measurement.

---

<sup>1</sup> The small residual error can be easily corrected with a small FIR filter if necessary.

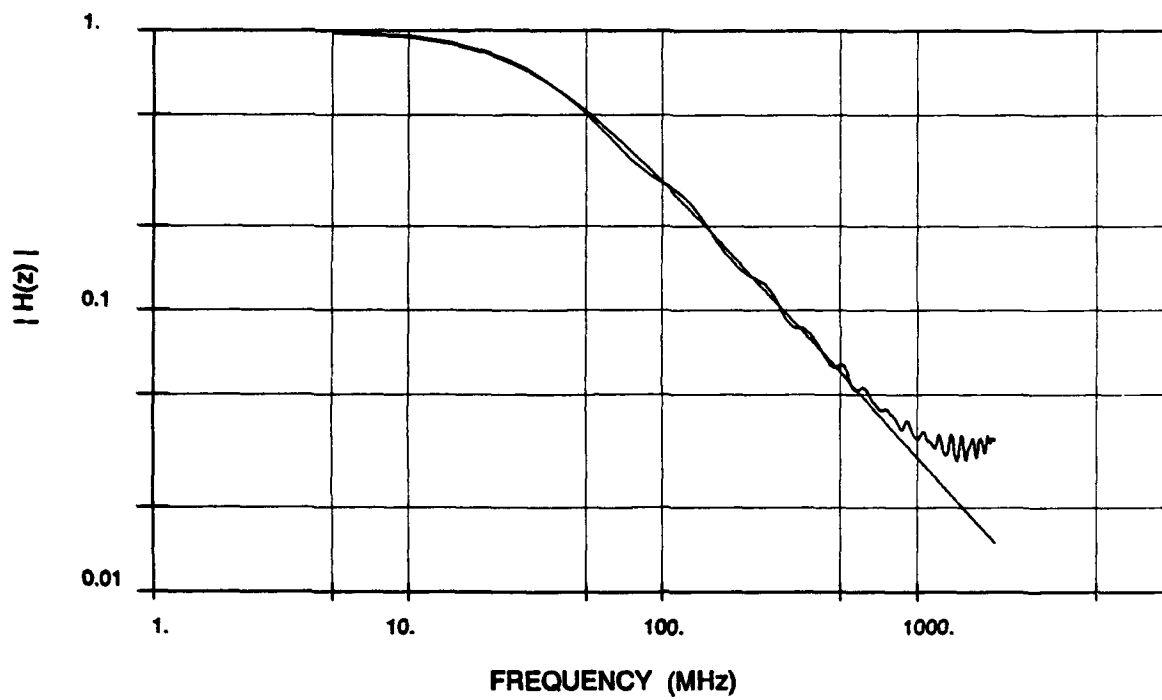


Figure 3-3. Frequency response of the partial-integrator.

### 3.2 COMPENSATING FOR LOW FREQUENCY CUT-OFF

It was shown that passive sensors connected to 50  $\Omega$  lines gives the time-derivative of the fields. However, if we consider the case of a small short-circuited loop, it is possible to obtain magnetic fields directly by measuring the current. Equation (20) then becomes  $I_{out} \approx A_{eq} \cdot B/L$ . This response is no longer dependent of the geometry alone and the sensor must be properly calibrated. The main parameter of the loop, beside its equivalent area, is its inductance, which is given by:

$$L = \mu_0 r \ln(8 \frac{r}{d} - 2) \quad (26)$$

which for small loops is of the order of 0.1  $\mu H$ . The DC resistance of the loop is negligible compared to the impedance of the probe. A current probe is basically a transformer whose primary is the wire carrying the current to measure. Typical current probes have an insertion impedance of 20 to 50 m $\Omega$ .

The values of R and L will effectively impose a low frequency cut-off at  $f_c = R/2\pi L$ , in the range of 30 to 300 kHz. The effect of this cut-off can be seen on Figure 3-4. The excitation (reference curve) is an ideal EMP waveform, with a rise-time of 6.5 ns, a pulse width of 266 ns and duration of about 1  $\mu s$ , matching the EMP simulator characteristics. Not surprisingly, the sensor will give an accurate measurement of the rising edge, but the falling edge will be affected by the cut-off. The waveform crosses the zero-axis at a earlier time and converges back to zero from the negative side.

Manufacturers of field sensors suggest a method to correct this distortion [11], but it is derived from integrals in their continuous form, which is not very practical. Instead, the correction may be achieved by using the IIR filter equivalent of  $(s+2\pi f_c)/s$ , yielding to:

$$y_n = y_{n-1} + (2\pi f_c \frac{T}{2} + 1) x_n - (2\pi f_c \frac{T}{2} - 1) x_{n-1} \quad (27)$$

Numerical error may be introduced for lower value of  $f_c$  or T because the coefficient of  $x_n$  and  $x_{n-1}$  then become very close to unity. This problem can be overcome by using double precision arithmetic.

As noted, it is necessary to calibrate the sensor, in particular to find the value of  $f_c$ . It is not always possible to measure the sensor response for very low frequencies<sup>1</sup>. It is however possible to obtain this value from a time

---

<sup>1</sup> For instance, the HP8753 network analyzer used for sensor calibration covers the band from 300 kHz to 6 GHz.



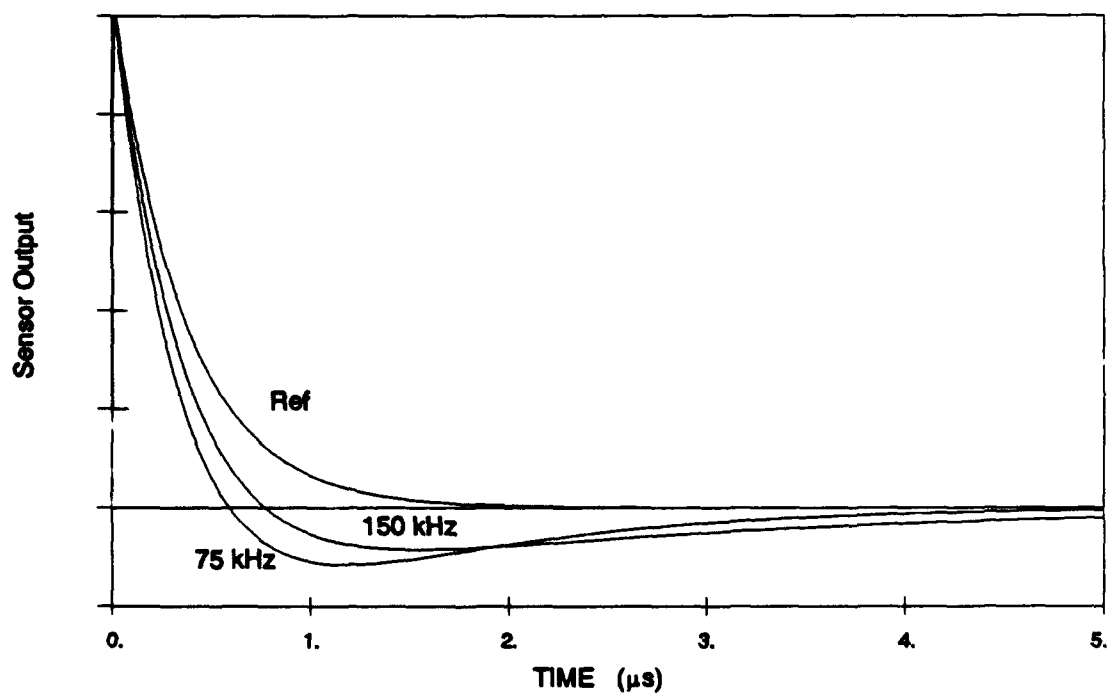


Figure 3-4. Effect of the low frequency cut-off of a sensor.

domain measurement. As seen on Figure 3-4, the sensor output crosses zero at a time  $t_0$  and this value is related to  $f_c$ . For  $t_0$  much larger than the rise time, the reference curve may be approximated by  $e^{-\alpha t}$  (from equation (1), where  $\beta \gg \alpha$ ) and the value of  $\alpha$  can be obtained from the curve. Solving the Laplace equation yield to:

$$\alpha e^{-t_0} = \omega_c e^{-\omega_c t_0} \quad (28)$$

which can be solved numerically by an iterative procedure.

#### 4.0 CORRECTING FOR MEASUREMENT SYSTEM ERRORS

Beside specific transfer functions and errors introduced by the sensors, the other components used in making the measurement system (cables, fiber optic links, digitizers, etc.) also introduce errors. Many of these errors can be precisely measured and an appropriate filter to compensate their effect can be designed.

The first section addresses the problem of losses in long cables. A technique is developed to design FIR filters of arbitrary transfer functions. Although the problem with cables is not severe, the same technique is used whenever a precise filter is required, such as in the case to fine tune an IIR filter.

The second section treats the problem of designing a digital filter when only the desired magnitude is known. The Hilbert transform is introduced to relate the magnitude and the phase response of a system.

#### 4.1 CORRECTING FOR CABLE LOSSES

The DREO large EMP simulator has a test area of 30 by 20 meters located about 15 m from the shielded room housing the instrumentation. Therefore, analog data links (coaxial cables or fiber optic) of up to 40-50 meters may be needed. Even good quality cables fitted with good quality connectors attenuate the higher frequencies by as much as 3 to 6 dB. This section describes the design of a corrective filter to compensate for this effect.

Figure 4-1 shows the frequency response,  $H(\omega)$ , of a 30 m cable. The apparently erratic behaviour of the phase is in fact a nearly linear phase, but with a rapid slope due to the long delay introduced by 30 m of cable<sup>1</sup>. This delay does not affect the solution and it can be removed easily (see below). The inverse of this response,  $H_c(\omega) = 1/H(\omega)$ , is used to compute the recovery filter. In this case, a FIR design was chosen to build the filter as it allows to model arbitrary transfer functions. The procedure is based on truncating the impulse response,  $h(n)$ , obtained from the inverse FFT of the frequency response. The truncation is performed by keeping all the points around the peak until  $h(n)$  permanently stay below a predetermined threshold, usually 0.1% to 1% of the peak. This procedure is valid if the sequence obtained is much shorter than the size of the FFT, which is the case if the filter results in fewer than 50 coefficients and a FFT size of 512 to 2048 is used. Because the frequency response is very

---

<sup>1</sup> In fact, when measuring the response of long cables with the HP8753 network analyzer, a very slow sweep should be chosen to remove the transient effect of the long delay.

smooth, the Gibbs phenomenon is negligible and the use of a window function is not necessary.

It is known that the straight application of the DFT way gives erroneous results. This subject has been treated extensively in the literature (such as [9], [12], [13], [14] and [17]) and will not be reviewed here.

The Fourier transform of a real signal yield to a symmetry between the positive and negative frequencies:  $G(f) = G^*(-f)$ . Consequently, it is necessary to supply both positive and negative frequencies to recover a real signal from its spectrum. The DFT of a  $N$ -point sequence, from  $t=0$  to  $(N-1)\Delta t$ , results in a sequence of  $N/2+1$  frequencies, from  $f=0$  to  $N/2 \cdot \Delta f$ , followed by its conjugate image,  $N/2-1$  frequencies, from  $f=-(N/2-1)\Delta f$  to  $-\Delta f$ <sup>1</sup>. It is therefore necessary to mirror the frequency response with its conjugate before taking its IDFT to obtain a real result. In addition, it is necessary that the response for  $f=0$  and  $f=(N/2)\Delta f$  be real (these are the only two frequencies which do not have their conjugate mirrored). The value at DC is always real and can be obtained from DC measurement or obtained by extrapolating the first few frequencies to zero. The value at  $f=N/2\Delta f$  however is generally complex. One possible work-around is to use a window function such as a cosine-taper to force the frequency response to zero or unity at that frequency. An other solution is to multiply the frequency response with the ideal delay line  $e^{-j\omega t_d}$ . This function has a unit magnitude and a linear phase, corresponding to a shift of the time domain respond by  $t=t_d$ . Choosing  $t_d$  to obtain a response of -1 at  $f=N/2\Delta f$ , ensures that the IDFT yields to a real result, and furthermore ensures that the phase will be continuous, ie. will not jump from a negative to a positive phase at that frequency.

Of course, the impulse response  $h(n)$  must be computed with the same sampling rate as the sequences to be filtered, which is determined by the specific digitizer used. For the HB7912 or SCD1000 for instance, the sampling rate is related to the time base as:  $\Delta T = 10t_{sw}/N_t$ , where  $t_{sw}$  is the sweep rate in second per division and  $N_t$  is the number of points (512 or 1024). The corresponding  $\Delta f$  required is:  $\Delta f = 1/(N_f \Delta T) = N_t/N_f / 10t_{sw}$ , where  $N_f$  is the size of the FFT. An appropriate value for  $\Delta f$  is 5 MHz, for sweep rates of the order of 10 nsec/div. It is not necessary to measure the cable characteristics for all possible values of  $\Delta f$ ; instead, decimation or interpolation of only few measurements may be done.

Figure 4-2 shows the function  $H_c(f)$  to compensate for the cable losses. A typical measurement with the HP8753 network analyzer is made at 401 frequencies, and with a  $\Delta f$  of 5 MHz, it covers a band up to 2 GHz. In this example, the coefficients are computed for a 10 ns/div sweep ( $\Delta T = 0.195$  ns) and for a FFT

<sup>1</sup> The DFT of a sequence is periodic itself, with a period of  $1/\Delta T$ . Therefore, the negative frequencies  $-(N/2-1)\Delta f$  to  $-\Delta f$  are reflected to  $(N/2+1)\Delta f$  to  $(N-1)\Delta f$ .

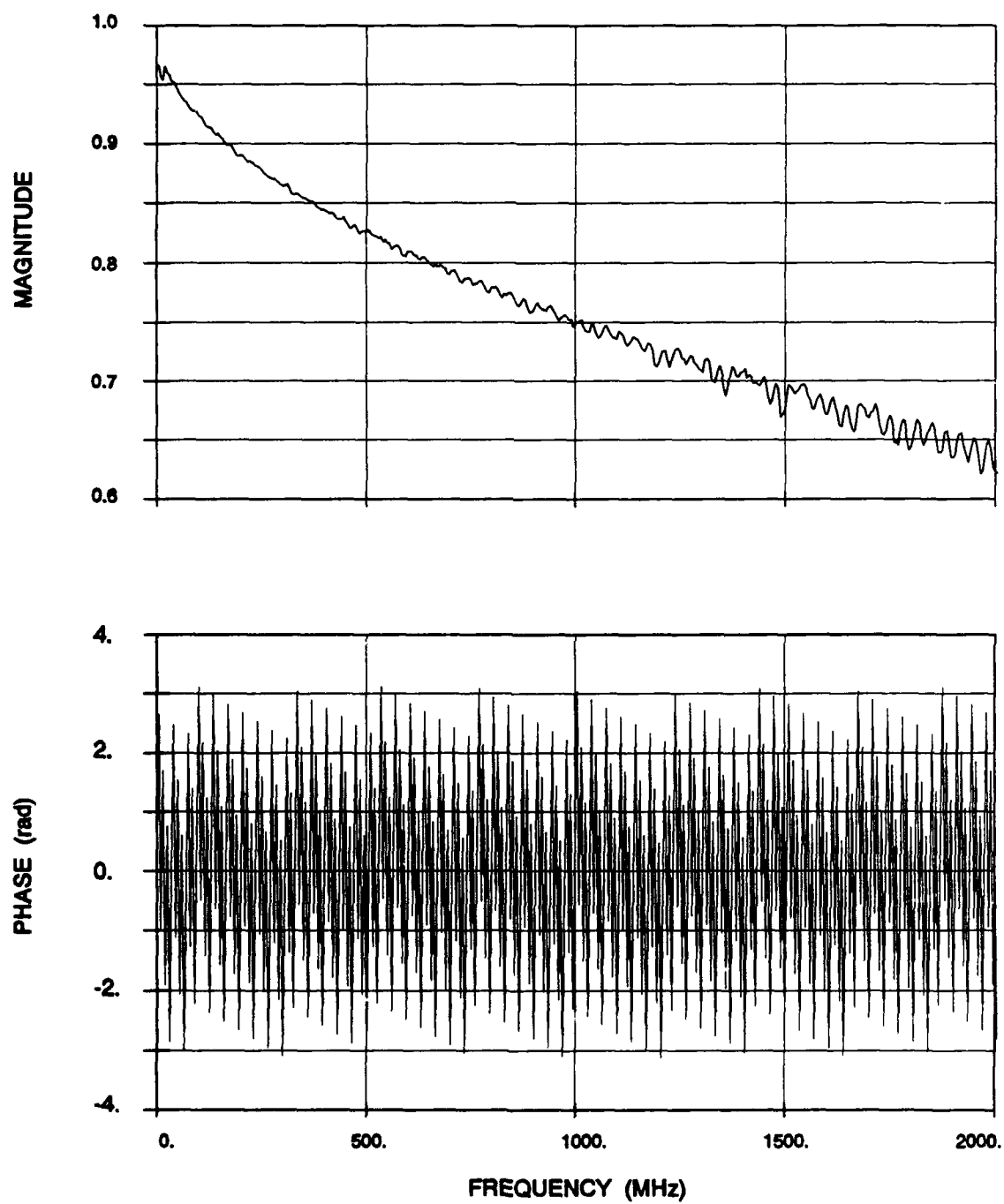


Figure 4-1. Frequency response of a 30 meter cable.

size of 1024. Therefore, it is necessary to specify  $H_c(f)$  up to 2.5 GHz and some extrapolation is required. One solution is to use a window function and force  $H_c$  to converge toward zero, let say in the band of 1.5 to 2 GHz. This is adequate if we consider that most of the signal is concentrated below 1 GHz and anything above is considered as noise. Another solution is to extrapolate  $H_c(f)$  either numerically (linear or quadratic) or by modelling it as a 1<sup>st</sup> or 2<sup>nd</sup>-order system. However, this method may produce unstable filters as the noise present in the higher frequencies will be amplified (correcting for losses of 3 to 6 dB generally produce good results, but great caution should be exercised for correction of more than 10 dB). The method used in this example, is to extend  $H_c(f)$  based on the value of the last frequencies present in the measurement. Its overall performances are good as the amount of boosting is limited and it tends to produce filters with fewer coefficients.

An impulse response obtained from the IDFT is also periodic, ie. a circular sequence is obtained. Due to inherent or added delays, the origin of the response is not necessarily the beginning or the middle of the sequence. The easiest procedure is to perform a circular shift to bring the peak value near the middle, then perform the truncation and possibly multiply with a window function. Figure 4-3 shows the function  $h(t)$  obtained from  $H_c(f)$  on Figure 4-2 (only about 80 coefficients are shown). By using a threshold of 1% of the peak value, this sequence can be truncated to 9 coefficients. The exact frequency response of this FIR filter is also compared with  $H_c(f)$  on Figure 4-2. The agreement is very good with an error smaller than 0.2 dB.

## 4.2 HILBERT TRANSFORM

In the previous section, a technique for designing a filter matching a given transfer function  $H(\omega)$  was presented. It relied on the full definition of  $H(\omega)$ , ie. both its real and imaginary components (or alternatively both magnitude and phase). Filters are frequently defined in terms of magnitude or squared-magnitude, and in many cases, it is difficult or not practical to measure both components. For instance, with the use of a sine-wave generator and a power meter, it is easy to measure the magnitude of the response of a digitizer, but not possible to obtain the phase information. The phase response cannot be simply ignored if a stable and causal system is desired.

Linear systems theory ([7], [9], [15], [18]) shows that for stable and causal systems, the real and imaginary parts of the Fourier transform are related to each other by the Hilbert transform. In particular, for minimal phase systems<sup>1</sup>, the following relation for  $H(\omega) = H_R(\omega) + jH_I(\omega)$  is obtained:

---

<sup>1</sup> A minimal phase system is one for which all the poles and zeros of the transfer function  $H(z)$  are inside the unit circle.

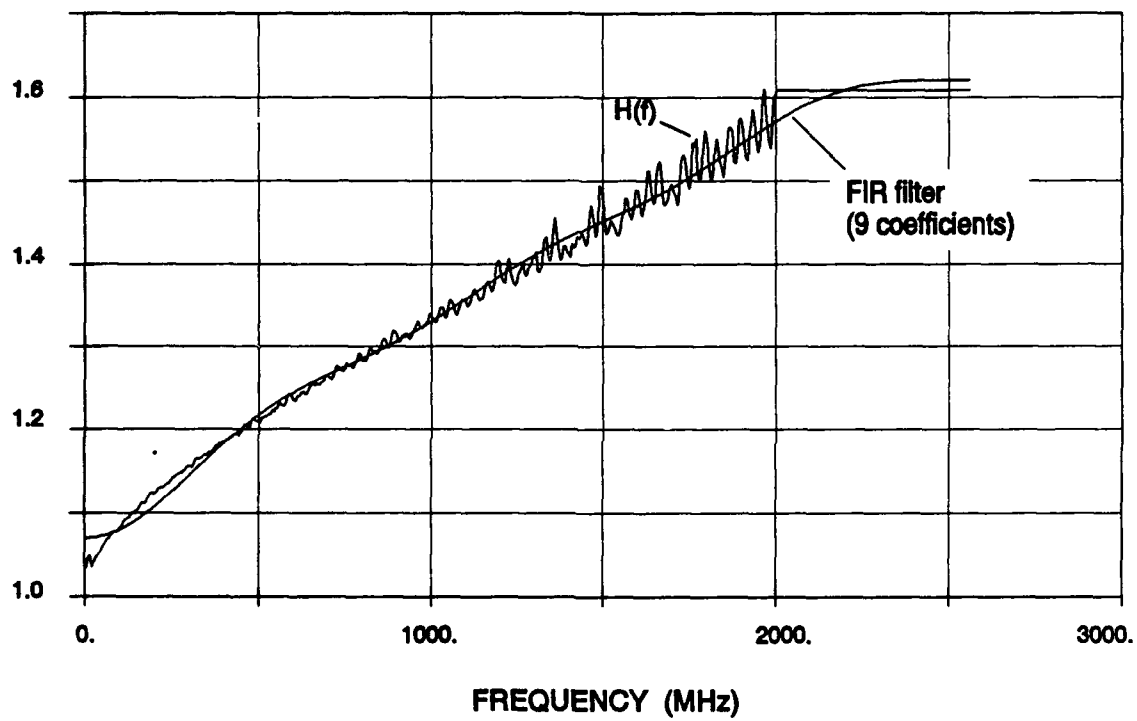


Figure 4-2. Response of filter for compensating cable losses.

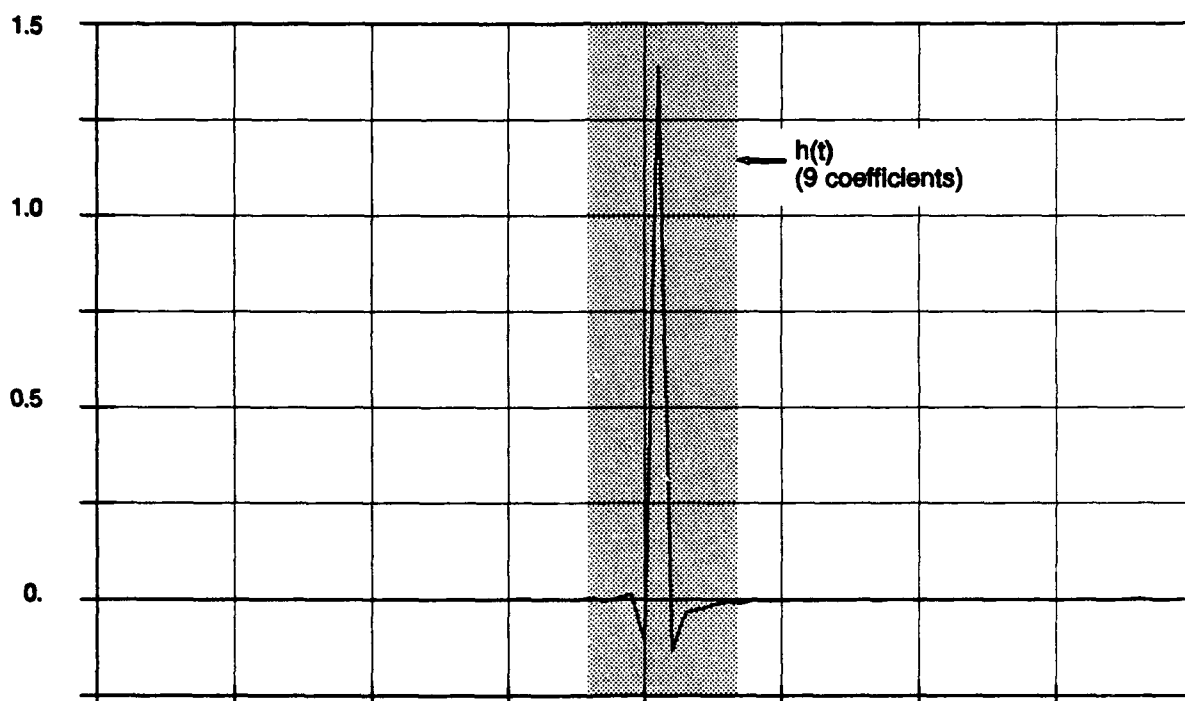


Figure 4-3. Impulse response of filter to compensate cable losses.



$$\begin{aligned} H_3(\omega) &= -\check{H}_2(\omega) \\ H_2(\omega) &= \check{H}_3(\omega) \end{aligned} \quad (29)$$

where  $\check{H}$  denotes the Hilbert transform of  $H$ . Similarly, the relation between the magnitude and phase can be easily demonstrated if we define  $H'(\omega)$  as the logarithm of  $H(\omega)$ , we obtain:

$$\begin{aligned} H'(\omega) &= \ln(|H(\omega)| \cdot e^{j\phi(\omega)}) \\ &= \ln|H(\omega)| + j\phi(\omega) \end{aligned} \quad (30)$$

which can be related to (29).

As with the Fourier transform, a discrete Hilbert transform (DHT) can be defined. However, it is easier and more efficient to relate the DHT with the DFT. The properties of the Hilbert transform are developed in [15], but the most important ones are summarized here:

The Hilbert transform  $\check{g}(t)$  of a real signal  $g(t)$  is real.

The duality property states that if the Hilbert transform of a signal  $g(t)$  is  $\check{g}(t)$ , then the Hilbert transform of  $\check{g}(t)$  is  $-g(t)$ .

And more important, the Fourier transforms of  $g(t)$  and  $\check{g}(t)$  are related as:

$$\check{G}(f) = -j \operatorname{sgn}(f) G(f) \quad (31)$$

where  $\operatorname{sgn}(f)$  is the signum function. This relation allows implementation of the DHT simply by using the already developed DFT or FFT algorithms.

For a sequence of  $N$  points formed from a signal and its mirrored conjugate, the signum function is defined as:

$$\operatorname{sgn}(n) = \begin{cases} 1 & \text{for } n = 1, 2, \dots, \frac{N}{2} \\ -1 & \text{for } n = \frac{N}{2}+1, \dots, N-1 \\ 0 & \text{for } n = 0, \frac{N}{2} \end{cases} \quad (32)$$

From the properties presented above, a simple procedure can be established to recover the phase information from the magnitude alone:

Form a N-point sequence  $\{x\}$  of the magnitude

Take the natural logarithm of  $\{x\}$

Mirror  $\{x\}$  with its conjugate, thus obtain an extended sequence  $\{x_m\}$  of M-points.

Take the FFT of  $\{x_m\}$

Multiply with  $\text{sgn}(n)$ , then with  $-j$

Take the real part of the inverse FFT

Truncate back to N-point

The example shown on Figure 4-4 illustrates this technique. The phase of a resonating 2<sup>nd</sup>-order system is reconstructed from its magnitude, shown on top. Due to the periodic nature of the DFT, the phase obtained converges back to zero at the maximum frequency, but as demonstrated in the previous section, this can be interpreted as a fixed amount of delay which has no effect on the design of a FIR filter. After compensating for that delay, the phase obtained with the Hilbert transform is in good agreement with the known phase.

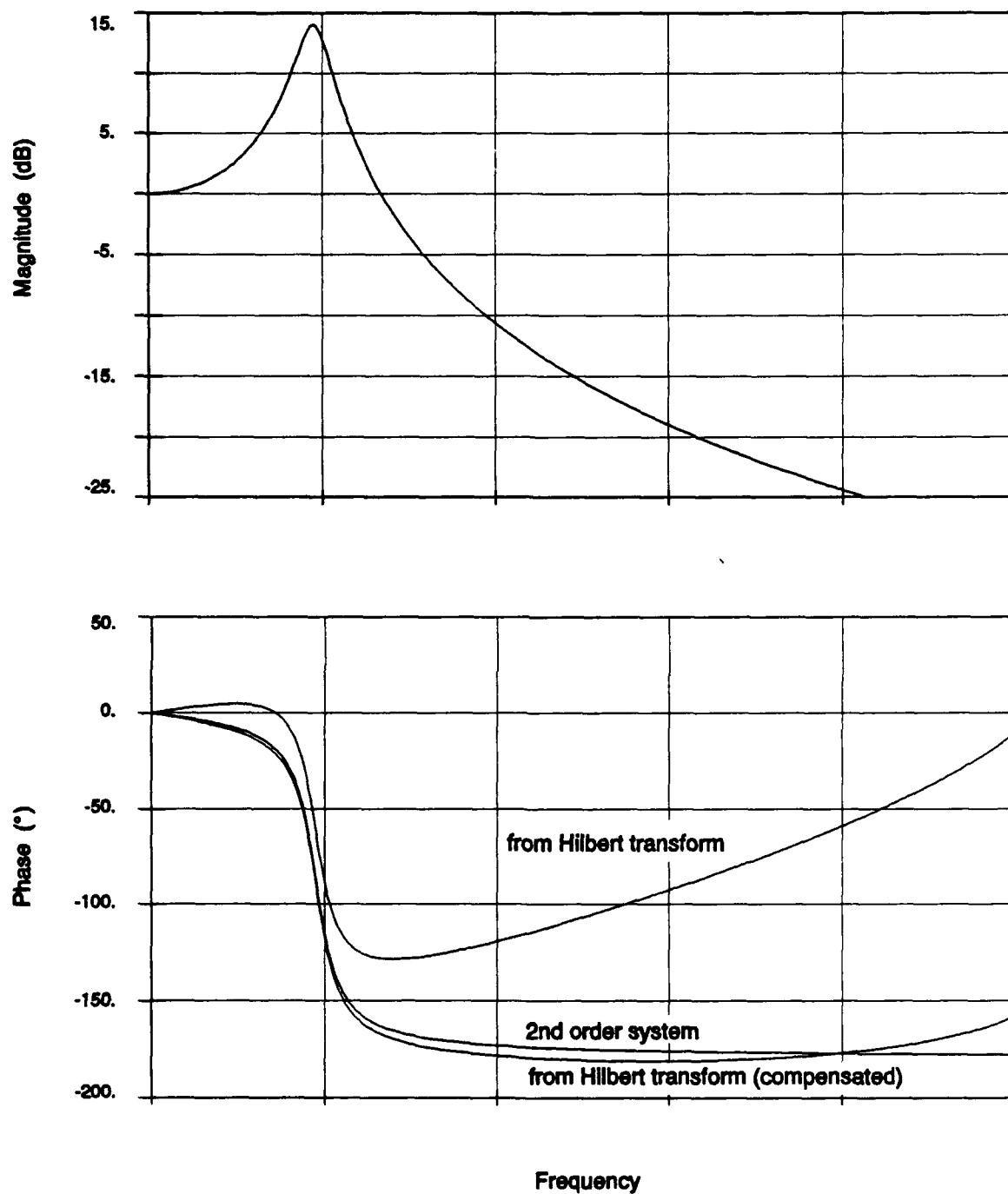


Figure 4-4. Use of the Hilbert transform for phase recovery.

## 5.0 CONCLUSION

It was shown that proper digital signal processing can significantly improve the accuracy of the measurements or extend the useful bandwidth or range of an instrument. Algorithms were developed to take into account the transfer functions inherent to each of the various sensors. Other techniques were developed to compensate for errors present in the measurement system.

It is necessary to integrate the output of electromagnetic field sensors responding to the time-derivative of the field. An alternative approach to perform this integration was developed. A specially made device (called a partial integrator) was designed and used in conjunction with digital filtering. Results showed that the bandwidth of the digitizers was extended by allowing the use of slower sweep rates, and that the dynamic range was extended by compressing the peak of the output and thus expanding the other portions of the waveform.

It was shown that some field sensors may be used to measure the field directly (and not the time-derivative). These measurements are affected by a low frequency cut-off and an algorithm was developed to compensate this effect.

A technique for designing FIR filters with arbitrary transfer function was introduced. This technique is particularly well suited to model the effect of signal transmission through long cables and also to fine tune the response of IIR filters. In many cases, very good response (error less than a fraction of a dB) can be obtained with few filter coefficients (between 10 to 50).

The relation between the Hilbert transform and the real and imaginary parts of a transfer function was presented. This relation was extended to relate both the magnitude and phase of the function, thus allowing to reconstruct the phase information from the magnitude alone. This relation allows the design of a FIR filter to model a system for which only the magnitude can be measured. A practical implementation of the discrete Hilbert transform was also presented.

## REFERENCES

- [1] K.S.H. Lee, *"EMP Interaction, Principles, Techniques, and Reference Data"*, Hemisphere Publishing Corporation, 1986
- [2] R.N. Ghose, *"EMP Environment and System Hardness Design"*, Don White Consultants, 1984
- [3] MIL-STD-461C, *"Electromagnetic Emission and Susceptibility Requirements for the Control of electromagnetic Interference"*, August 1986
- [4] NATO, *"EMP engineering practices handbook"*, NATO file No 1460-3, August 1988
- [5] NATO, *"The NATO User Guide to EMP Testing and Simulation"*, AEP-18, 1<sup>st</sup> edition, July 1988
- [6] Bell Laboratories, *"EMP engineering and design principles"*, 1975
- [7] A.V. Oppenheim and R.W. Schaffer, *"Digital Signal Processing"*, Prentice-Hall, 1975
- [8] A.V. Oppenheim and A.S. Willsky, *"Signals and Systems"*, Prentice-Hall, 1983
- [9] L.R. Rabiner and B. Gold, *"Theory and Application of Digital Signal Processing"*, Prentice-Hall, 1975
- [10] E.K. Miller, *"Time-Domain Measurements in Electromagnetics"*, Van Nostrand Reinhold, 1986
- [11] *"Integrator Correction"*, EG&G, Data Sheet 1007, July 1981
- [12] D.F. Elliott and K.R. Rao, *"Fast Transforms - Algorithms, Analyses, Applications"*, Academic Press Inc., 1982
- [13] C.S. Burrus and T.W. Parks, *"DFT/FFT and Convolution Algorithms"*, John Wiley & Sons, 1985
- [14] G.D. Bergland, *"A Guided Tour of the Fast Fourier Transform"*, IEEE Spectrum, Vol. 6, July 1969
- [15] S. Haykin, *"Communication Systems"*, John Wiley & Sons, 1978
- [16] S. Kashyap, J.S. Seregelyi and M. Dion, *"Measurement of EMP Transients Using a Small, Parallel Plate Simulator"*, Proceedings of the IEEE Conference on Precision Electromagnetic Measurements, June 11-14, 1990

- [17] M. Dion and S. Kashyap, "*Analysis of EMP Responses of Structures Using Frequency Domain Electromagnetic Interaction Codes*", DREO report 1078, May 1991
- [18] B. Gold, A.V. Oppenheim, C.M. Rader, "*Theory and Implementation of the Discrete Hilbert Transform*", Symposium on Computer Processing in Communication, April 1969
- [19] V. Čížek, "*Discrete Hilbert Transform*", IEEE Transactions on Audio and Electroacoustics, Vol. AU-18, No. 4, December 1970

UNCLASSIFIED

-37-

SECURITY CLASSIFICATION OF FORM  
(highest classification of Title, Abstract, Keywords)

**DOCUMENT CONTROL DATA**

(Security classification of title, body of abstract and indexing annotation must be entered when the overall document is classified)

|   |  |   |  |
|---|--|---|--|
| <b>1. ORIGINATOR</b> (the name and address of the organization preparing the document. Organizations for whom the document was prepared, e.g. Establishment sponsoring a contractor's report, or tasking agency, are entered in section 8.)<br>Defence Research Establishment Ottawa<br>Ottawa, Ontario<br>K1A 0Z4  |  | <b>2. SECURITY CLASSIFICATION</b><br>(overall security classification of the document including special warning terms if applicable)<br><br><b>UNCLASSIFIED</b> |  |
| <b>3. TITLE</b> (the complete document title as indicated on the title page. Its classification should be indicated by the appropriate abbreviation (S,C or U) in parentheses after the title.)<br><br>DESIGN OF DIGITAL SIGNAL PROCESSING ALGORITHMS FOR ENHANCING THE MEASUREMENTS OF ULTRA-FAST ELECTROMAGNETIC TRANSIENTS (U)   |  |   |  |
| <b>4. AUTHORS</b> (Last name, first name, middle initial)<br>DION, MARC   |  |   |  |
| <b>5. DATE OF PUBLICATION</b> (month and year of publication of document)<br>DECEMBER 1991  |  | <b>6a. NO. OF PAGES</b> (total containing information. Include Annexes, Appendices, etc.)<br>42   | <b>6b. NO. OF REFS</b> (total cited in document)<br>19 |
| <b>7. DESCRIPTIVE NOTES</b> (the category of the document, e.g. technical report, technical note or memorandum. If appropriate, enter the type of report, e.g. interim, progress, summary, annual or final. Give the inclusive dates when a specific reporting period is covered.)<br>DREO Report   |  |   |  |
| <b>8. SPONSORING ACTIVITY</b> (the name of the department project office or laboratory sponsoring the research and development. Include the address.)<br>DREO<br>3701 CARLING AVE<br>OTTAWA, ONTARIO K1A 0K2  |  |   |  |
| <b>9a. PROJECT OR GRANT NO.</b> (if appropriate, the applicable research and development project or grant number under which the document was written. Please specify whether project or grant)<br>PROJECT 041LT  |  | <b>9b. CONTRACT NO.</b> (if appropriate, the applicable number under which the document was written)  |  |
| <b>10a. ORIGINATOR'S DOCUMENT NUMBER</b> (the official document number by which the document is identified by the originating activity. This number must be unique to this document.)<br>DREO REPORT 1095   |  | <b>10b. OTHER DOCUMENT NOS.</b> (Any other numbers which may be assigned this document either by the originator or by the sponsor)                              |  |
| <b>11. DOCUMENT AVAILABILITY</b> (any limitations on further dissemination of the document, other than those imposed by security classification)<br><br><input checked="" type="checkbox"/> (X) Unlimited distribution<br><input type="checkbox"/> ( ) Distribution limited to defence departments and defence contractors; further distribution only as approved<br><input type="checkbox"/> ( ) Distribution limited to defence departments and Canadian defence contractors; further distribution only as approved<br><input type="checkbox"/> ( ) Distribution limited to government departments and agencies; further distribution only as approved<br><input type="checkbox"/> ( ) Distribution limited to defence departments; further distribution only as approved<br><input type="checkbox"/> ( ) Other (please specify): |  |   |  |
| <b>12. DOCUMENT ANNOUNCEMENT</b> (any limitation to the bibliographic announcement of this document. This will normally correspond to the Document Availability (11). however, where further distribution (beyond the audience specified in 11) is possible, a wider announcement audience may be selected.)<br>Unlimited Announcement  |  |   |  |

UNCLASSIFIED

SECURITY CLASSIFICATION OF FORM

RA.W (17 Dec 90)

## UNCLASSIFIED

SECURITY CLASSIFICATION OF FORM  
(highest classification of Title, Abstract, Keywords)

## DOCUMENT CONTROL DATA

(Security classification of title, body of abstract and indexing annotation must be entered when the overall document is classified)

|  |   |   |  |
|--|---|---|--|
| <b>1. ORIGINATOR</b> (the name and address of the organization preparing the document. Organizations for whom the document was prepared, e.g. Establishment sponsoring a contractor's report, or tasking agency, are entered in section 8.)<br>Defence Research Establishment Ottawa<br>Ottawa, Ontario<br>K1A 0Z4   |   | <b>2. SECURITY CLASSIFICATION</b><br>(overall security classification of the document including special warning terms if applicable)<br><br><b>UNCLASSIFIED</b> |  |
| <b>3. TITLE</b> (the complete document title as indicated on the title page. Its classification should be indicated by the appropriate abbreviation (S,C or U) in parentheses after the title.)<br><br><b>DESIGN OF DIGITAL SIGNAL PROCESSING ALGORITHMS FOR ENHANCING THE MEASUREMENTS OF ULTRA-FAST ELECTROMAGNETIC TRANSIENTS (U)</b>   |   |   |  |
| <b>4. AUTHORS</b> (Last name, first name, middle initial)<br>DION, MARC  |   |   |  |
| <b>5. DATE OF PUBLICATION</b> (month and year of publication of document)<br>DECEMBER 1991   | <b>6a. NO. OF PAGES</b> (total containing information. Include Annexes, Appendices, etc.)<br>42 | <b>6b. NO. OF REFS</b> (total cited in document)<br>19  |  |
| <b>7. DESCRIPTIVE NOTES</b> (the category of the document, e.g. technical report, technical note or memorandum. If appropriate, enter the type of report, e.g. interim, progress, summary, annual or final. Give the inclusive dates when a specific reporting period is covered.)<br>DREO Report  |   |   |  |
| <b>8. SPONSORING ACTIVITY</b> (the name of the department project office or laboratory sponsoring the research and development. Include the address.)<br>DREO<br>3701 CARLING AVE<br>OTTAWA, ONTARIO K1A 0K2   |   |   |  |
| <b>9a. PROJECT OR GRANT NO.</b> (if appropriate, the applicable research and development project or grant number under which the document was written. Please specify whether project or grant)<br>PROJECT 041LT   |   | <b>9b. CONTRACT NO.</b> (if appropriate, the applicable number under which the document was written)  |  |
| <b>10a. ORIGINATOR'S DOCUMENT NUMBER</b> (the official document number by which the document is identified by the originating activity. This number must be unique to this document.)<br>DREO REPORT 1095  |   | <b>10b. OTHER DOCUMENT NOS.</b> (Any other numbers which may be assigned this document either by the originator or by the sponsor)                              |  |
| <b>11. DOCUMENT AVAILABILITY</b> (any limitations on further dissemination of the document, other than those imposed by security classification)<br><br>(X) Unlimited distribution<br>( ) Distribution limited to defence departments and defence contractors; further distribution only as approved<br>( ) Distribution limited to defence departments and Canadian defence contractors; further distribution only as approved<br>( ) Distribution limited to government departments and agencies; further distribution only as approved<br>( ) Distribution limited to defence departments; further distribution only as approved<br>( ) Other (please specify): |   |   |  |
| <b>12. DOCUMENT ANNOUNCEMENT</b> (any limitation to the bibliographic announcement of this document. This will normally correspond to the Document Availability (11). however, where further distribution (beyond the audience specified in 11) is possible, a wider announcement audience may be selected.)<br>Unlimited Announcement   |   |   |  |

UNCLASSIFIED

SECURITY CLASSIFICATION OF FORM

RA.W (17 Dec 90)